Effect of 180° bends on gas/liquid flows in vertical upward and downward pipes

A. Almabrok, L. Lao & H. Yeung
Department of Offshore, Process and Energy Engineering, Cranfield University, UK

Abstract

Experimental investigation has been carried out on upward and downward vertical pipes with 180° bends to study gas-liquid two-phase flow behaviours in pipes with serpentine configuration. Wire mesh sensor (WMS) is installed at top and bottom positions of upward and downward sections in order to identify the void fraction distributions. Film thickness probes are employed to obtain circumferential profile of the liquid film thickness at different axial positions along both sections. Further features such as flow patterns are identified by examining the time trace and probability density function (PDF) data. All measurements are conducted for different superficial gas velocities, while superficial liquid velocity is fixed at 1.0 m/s.

The study identified that the centrifugal force present in 180° bends caused a flow maldistribution in the adjacent straight sections. It is noted from the time trace and PDF results that the superficial gas velocity has obvious effects on the flow development along different positions of the pipes, where the flow regime varied over whole velocity ranges tested. These results are confirmed by the cross-sectional view and sliced stack images (longitudinal view) of the void fraction distributions. The results also showed that the flow behaviour in upward and downward pipes is affected by bends, although to varying degrees.
Keywords: upward, downward, 180° bends, film thickness probes, WMS.

1 Introduction

Gas-liquid two-phase flows in serpentine vertical pipes connected together by 180° bends are of great importance in a wide range of engineering practices. The development of many new technologies such as the design of offshore gas and

WIT Transactions on Engineering Sciences, Vol 79,
www.witpress.com, ISSN 1743-3533 (on-line)
doi:10.2495/MPF130361

oil pipelines and the prediction of heat transfer characteristics for condensation/evaporation processes have been related to gas-liquid issues. Furthermore, in many industrial units such as a large cracking furnace in a refinery, the tubes are arranged in a serpentine manner and are relatively short. Thus, it is not clear how much effect the bends exert on the flow in the straight part of the tube. As flow negotiates round the 180° bend at the ends the generated centrifugal force could cause flow maldistribution creating local dry spots, where no steady liquid film formed on the pipe walls. As a result, events including coking, cracking and overheating of heat transfer surfaces, may occur and lead to frequent shutdown of the facilities. This could increase the operating costs and reduce production revenue.

However, a large amount of investigations such as that of Alves [1], Oshinowo and Charles [2], Usui *et al.* [3], Azzi *et al.* [4], Azzi and Friedel [5], Spedding and Benard [6] and Shannak *et al.* [7] are available in a literature. These investigations are limited to upward flow with small diameter pipe ranging from 5 to 50 mm. Reported literature on two-phase flow in 180° bends in large diameter pipes is scarce. Abdulkadir *et al.* [8] carried out an experimental study into the churn-annular flow behaviour to measure mean film fraction of air-water mixture through a vertical 180° return bend using electrical conductance tomography sensor. The study is distinctive in that it is probably the first major study in open literature on 180° bends utilising a large internal diameter (i.d. =127 mm) pipe. They measured film fraction using conductance ring probes positioned before the bend, within the bend (at 45°, 90°, 135° angles) and after the bend. They noted that the average film fraction is higher in the straight pipes than in the bends and that at low liquid/higher gas flow rates, film break up occurs at the 45° bend due to gravity drainage. They also reported that the flow behaviour round the bend is affected due to existence of centrifugal and gravitational forces.

The objective of the current work is to expand the understanding of flow behaviour in large diameter pipes connected together by 180° bends. The experimental investigation focused on the gas-liquid two-phase flow development in both upward and downward straight sections of pipes after a 180° bend.

2 Description of test facility and instrumentation

The serpent test facility (Figure 1) is specially designed and built in the Flow Laboratory at Cranfield University. The test facility is divided into three sections: the fluid supply and metering section, the test section and the separation section. This facility is controlled by data acquisition system which includes Delta-V and Labview systems. Water and air at measured rates are mixed through a T-junction then fed through the test section and finally exit into the ventilation tank where the water and air are separated. After separation the water flows back to its storage tank while the air is vented into the atmosphere. The test section consists of a flow loop of about 20 m long in total and 101.6 mm bore size pipeline which includes four vertical upward and

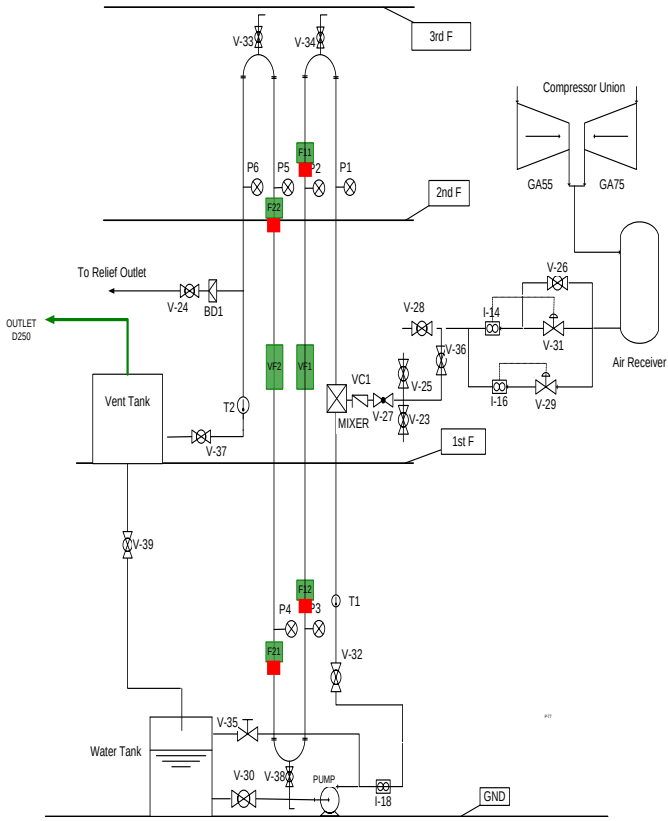

Figure 1: Schematic of test facility. The liquid film probes are shown in green colour and the wire mesh sensor is shown in red colour.

downward sections connected by three identical transparent 180° bends. The bend's centre line radius (CLR) is 203 mm. The locations of the liquid film probes are 4.91, 30.41 and 46.16 pipe diameters downstream and upstream of the top and bottom bends respectively. The film probes consist of four conductive sensors distributed circumferentially around the pipe, as shown in Figure 2. The sensing part of the conductivity film thickness probes compose of two stainless steel conductors arranged with the insulator between them. The end of the sensor is mounted flush with the inner surface of the pipe. Each conductor is electrically in contact with the liquid film when the liquid film flows over them so a conductive bridge is formed between them. The 32×32 capacitance WMS is installed at the top and bottom positions of downward and upward sections with axial distances 4.41 and 45.66 pipe diameters downstream and upstream of the top and bottom bends respectively. A more detailed description of this technique is presented by Da Silva *et al.* [9].

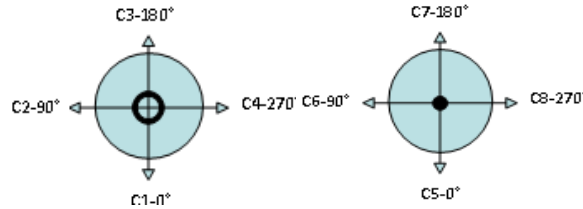

Figure 2: Circumferential positions of the sensors in film thickness probes at downward section (a) and upward section (b).

3 Procedure of the tests

The test section is first emptied and blown dry. The air flow is stopped to record the zero points of the instrumentation. The rig is then filled with water to record full scale output of liquid film probes. The water flow rate is adjusted to a predetermined value before air is introduced to the test section, and then the water flow rate is monitored and adjusted to keep it at the predetermined value while the air flow is slowly increased to the desired value. Finally, the test section is again emptied and blown dry to record the zero point of the instrumentation.

4 Results and discussion

The results from air-water two-phase flow tests are for the void fraction distributions and liquid film thickness in upward and downward flows. These results are expected to provide more knowledge about the gas void fraction distributions and liquid film profiles along different parts of the vertical pipes.

4.1 Flow regime and its development

In this study, the time trace, PDF and cross-sectional distributions of the void fraction are used to explore the effects of 180° bend on the flow regime and its development at various locations along the pipe. All results presented here are obtained at superficial gas velocities of 0.52 and 9.79 m/s, whilst the superficial liquid velocity is fixed at 1.0 m/s.

4.1.1 Downward flow

The time trace data illustrated in Figure 3(a) shows that the characteristic of waves at the top position is not similar to the bottom position. This is because the significant effects of the top bend on the void fraction characterises the top position. A large fluctuation of the flow is identified at the top position, due to the action of centrifugal force that is present in the bend, while the flow regime at the bottom position is confirmed to be a slug flow accompanied by huge waves as shown in Figure 4(a). The PDF shape represented in Figure 3(b) shows that unstable flow with a broad base is formed at the top position, for superficial

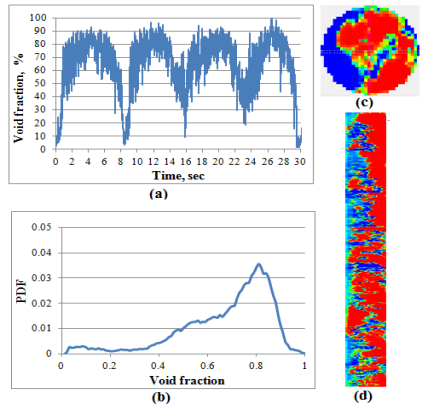

Figure 3: (a) time trace, (b) PDF, (c) cross-sectional view and (d) sliced stack image of the void fraction at the top position of downward, for superficial gas and liquid velocities of 0.52 and 1 m/s, respectively.

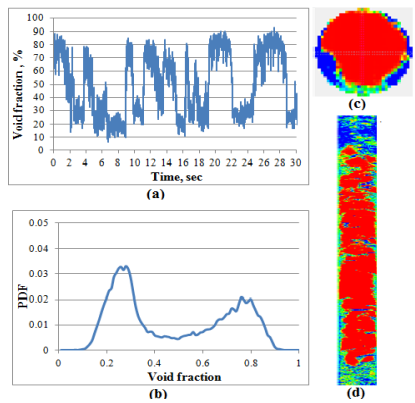

Figure 4: (a) time trace, (b) PDF, (c) cross-sectional view and (d) sliced stack image of the void fraction at the bottom position of downward, for superficial gas and liquid velocities of 0.52 and 1 m/s, respectively.

gas velocity of 0.52 m/s and superficial liquid velocity of 1.0 m/s. Slug flow is observed at the bottom position for the same conditions, as illustrated in Figure 4(b). The difference between the flow regimes at the top and lower positions is due to the effect of the top bend on the void fraction distributions at the top position. This effect diminishes as the flow reaches the bottom position. Figure 3(c) and (d) represents the cross-sectional view and sliced stack images of the void fraction distributions respectively, that are identified at the top position. In all images, the liquid phase is shown in blue colour while the gas phase is shown in red colour. The present study used these images as another approach to

interpret the flow regimes and its development along the pipe. It is important to mention that these images are applied to validate the time trace and PDF results. Figure 3(c) and (d) shows that an asymmetrical flow is identified at the top position, which is accompanied by a large number of liquid droplets entrained into the pipe centre (classified as wisps). This is due to the action of centrifugal force that acts to push the liquid phase into the outer curvature of the bend. On reaching the bottom position, the wisps become less and the flow is observed to be more symmetrical, as shown in Figure 4(c) and (d).

By increasing the superficial gas velocity further to 9.79 m/s, the time trace data at the top position shows that the height of waves is very large compared with those identified at the bottom position, as illustrated in Figures 5(a) and 6(a) respectively. This is because at the top position more bubbles are trapped in the pipe centre due to the action of the top bend. The PDF characteristic for the top and bottom positions shows annular flow formation, as illustrated in Figures 5(b) and 6(b) respectively. These results are confirmed by analysis of the cross-sectional view and sliced stack image of the void fraction distributions at both positions. Figure 5(c) and (d), confirmed that at the top position the annular flow is created with a large number of liquid droplets entrained into the pipe centre in the form of wisps. This is based on the fact that the centrifugal force present in the bend could cause a flow maldistribution in the adjacent straight sections, which is acting to push the liquid into the outer curvature of the bend. On the other hand, the flow becomes more uniformly distributed with less liquid entrainment when it has reached the bottom position, however it is still annular, as presented in Figure 6 (c) and (d). These observations are validated by the film thickness data obtained at the same position and for the same velocities, as shown in Figure 11(b).

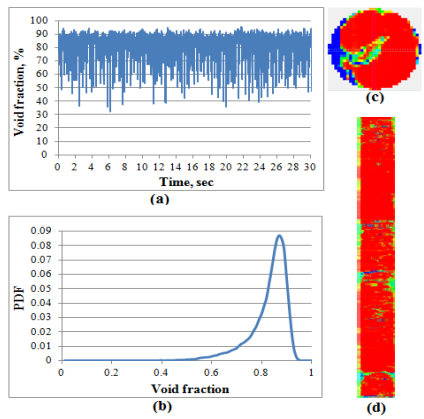

Figure 5: (a) time trace, (b) PDF, (c) cross-sectional view and (d) sliced stack image of the void fraction at the top position of downward, for superficial gas and liquid velocities of 9.79 and 1 m/s, respectively.

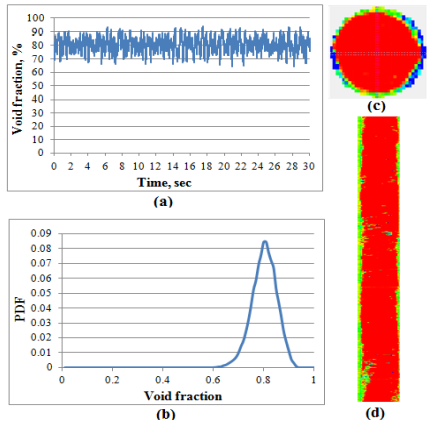

Figure 6: (a) time trace, (b) PDF, (c) cross-sectional view and (d) sliced stack image of the void fraction at the bottom position of downward, for superficial gas and liquid velocities of 9.79 and 1 m/s, respectively.

4.1.2 Upward flow

Figures 7 and 8 present a comparison between the bottom and top positions respectively, for (a) time trace, (b) PDF, (c) cross-sectional view and (d) sliced stack image of the void fraction. The comparison is made for superficial gas velocity of 0.52 m/s, whilst superficial liquid velocity is fixed at 1 m/s. Figures 7(a) and 8(a) show different signals between the time trace data obtained

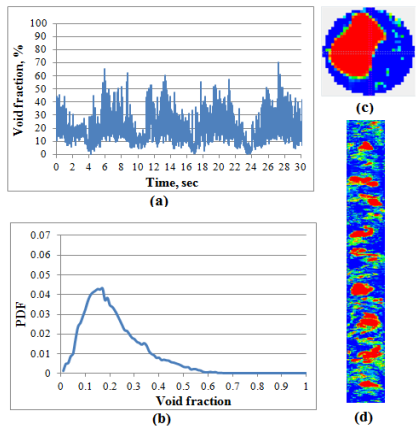

Figure 7: (a) time trace, (b) PDF, (c) cross-sectional view and (d) sliced stack image of the void fraction at the bottom position of upward, for superficial gas and liquid velocities of 0.52 and 1 m/s, respectively.

at the bottom and top positions respectively. The shape of PDF presented in Figure 7(b) confirms that the flow regime observed at the bottom position is bubbly to slug flow transition. The existence of large bubbles in a liquid phase contributed to the broad base. While, the shape of the PDF at top position is significantly different, which indicates a slug flow formation as presented in Figure 8(b). It can be noted from the cross-sectional view of the void fraction distribution and its sliced stack image shown in Figure 7(c) and (d) respectively, that the transition from bubbly to slug flow is confirmed at the bottom position. In contrast, Figure 8(c) and (d) shows that a slug flow accompanied by large bubbles (classified as Taylor bubbles) is formed at the top position.

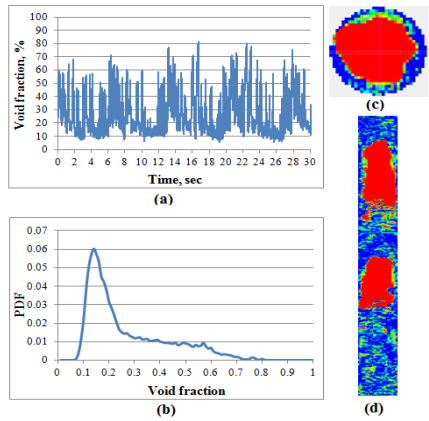

Figure 8: (a) time trace, (b) PDF, (c) cross-sectional view and (d) sliced stack image of the void fraction at the top position of upward, for superficial gas and liquid velocities of 0.52 and 1 m/s, respectively.

An examination of the time trace data at the bottom and top positions shows a similar tendency of the time trace signal when the superficial gas velocity is increased to 9.79 m/s, as illustrated in Figures 9(a) and 10(a) respectively. However, the time trace signal at the bottom position shows higher variations than that at the top position. The plots in Figures 9 (b) and 10(b) represent the PDF results obtained at the bottom and top positions respectively. It is clear from the plots that the PDF shapes did not show any discrepancies. Churn flow is observed for both positions with a broad base of void fraction values. These results are consistent with those obtained from the cross-sectional view and sliced stack image of the void fraction distribution. The flow profile at the bottom position is observed to be more evenly distributed than that at the top position. These results are in good agreement when compared with the circumferential distribution of liquid film, as shown in Figure 12(b).The film thickness at the bottom position is affected by the action of centrifugal force that exists in the bottom bend. On the contrary, the effect of this force is reduced when the flow reached the top position. This in turn led to create uniform liquid film profile around the cross section of the pipe.

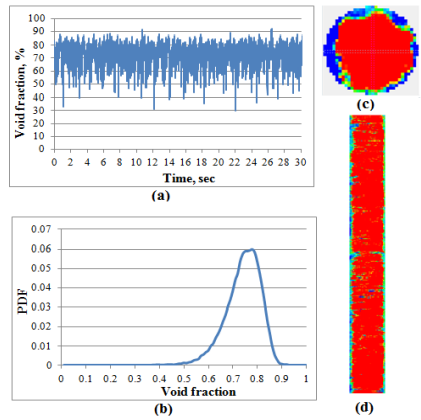

Figure 9: (a) time trace, (b) PDF, (c) cross-sectional view and (d) sliced stack image of the void fraction at the bottom position of upward, for superficial gas and liquid velocities of 9.79 and 1 m/s, respectively.

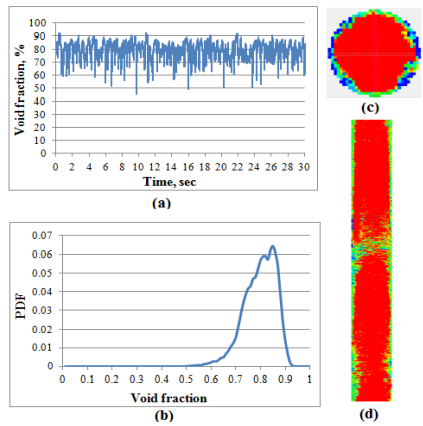

Figure 10: (a) time trace, (b) PDF, (c) cross-sectional view and (d) sliced stack image of the void fraction at the top position of upward, for superficial gas and liquid velocities of 9.79 and 1 m/s, respectively.

4.2 Circumferential distribution of the liquid film

In this study, circumferential distribution of liquid film is investigated along different positions of the pipe. Figures 11 and 12 below show the plots of the liquid film distribution at the top, middle and bottom positions of downward and upward sections respectively, for superficial gas velocities of 1.32 and 9.79 m/s respectively, while a superficial liquid velocity is fixed at 1.0 m/s.

4.2.1 Downward flow

It can be noted from the plots presented in Figure 11(a) and (b) that the liquid film thickness at 90° of the top position (corresponds to the sensor CT2 located in the outer curvature of the top bend) is thicker than other locations (0°, 180° and 270°) for the whole ranges of superficial velocities tested. This is due to the effect of the centrifugal force that observed to push the liquid into the outer curvature of the bend. The force effect diminishes when the flow reached the lower measuring positions. As a result, the liquid film profile at the middle and bottom positions are almost identical. It is worth mentioning that the top bend has no obvious effect on the middle and bottom positions even at higher superficial gas velocity, as shown in Figure 11(b).

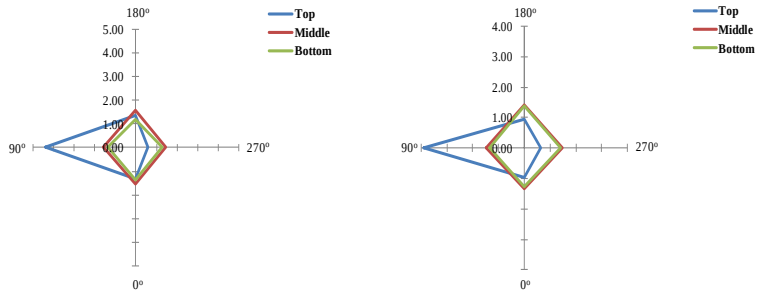

(a) (b)

Figure 11: Circumferential profile of the liquid film in downward at superficial gas velocities of 1.32 m/s (a) and 9.79 m/s (b), and superficial liquid velocity of 1 m/s. (Axes unit in all plots is mm).

4.2.2 Upward flow

Figure 12(a) shows that the film thickness distribution at the top, middle and bottom positions is systematically circumferentially uniform. However, the film thickness at the bottom position is notably thicker than those at the top and

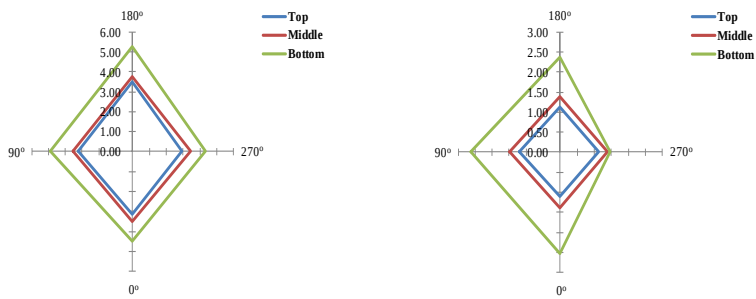

(a) (b)

Figure 12: Circumferential profile of the liquid film in upward at superficial gas velocities of 1.32 m/s (a) and 9.79 m/s (b), and superficial liquid velocity of 1 m/s. (Axes unit in all plots is mm).

middle positions. This evidence suggested that, at these conditions the centrifugal force action on the liquid film distributions is insignificant for all positions. With increasing the superficial gas velocity to 9.79 m/s, the film profile for the bottom position is considerably affected by the centrifugal force that is present in the bottom bend, as illustrated in Figure 12(b).

5 Conclusions

In this study, film thickness probes and WMS are applied to investigate the effects of 180° bends on behaviours of gas-liquid flows. The study found that the top and bottom bends have considerable impacts on the liquid film and void fraction profiles, to varying degrees. The action of these bends is highly dependent on the superficial gas velocity. The study also identified that the centrifugal force present in bends causes a flow maldistribution in the adjacent straight sections. From the time trace, PDF, cross-sectional view and sliced stack images of the void fraction distributions, it can be concluded that the superficial gas velocity has an obvious effect on the flow development along both orientations, where the flow regime varied over whole velocity ranges tested.

References

[1] Alves, G.E., Co-current liquid-gas flow in a pipeline contactor. *Chemical Engineering Progress*, **50**, pp. 449–456, 1954.
[2] Oshinowo, T. and Charles, M.E., Vertical two-phase flow–Part 1: Flow pattern correlations. *The Canadian Journal of Chemical Engineering*, **52**, pp. 25–35, 1974.
[3] Usui, K., Aoki, S., and Inoue, A., Flow behaviour and phase distributions in two-phase flow around inverted U-bend. *Journal of Nuclear Science and Technology*, **20**, pp. 915–928, 1983.
[4] Azzi, A., Friedel, L., Kibboua, R. and Shannak, B., Reproductive accuracy of two-phase flow pressure loss correlations for vertical 90 degree bends. *Forschung im Ingenieurwesen*, **67**, pp. 109–116, 2002.
[5] Azzi, A. and Friedel, L., Two-phase upward flow 90 degree bend pressure loss model. *Forschung im Ingenieurwesen*, **69**, pp. 120–130, 2005.
[6] Spedding, P.L., and Benard, E., Gas-liquid two-phase flow through a vertical 90 degree elbow bend. *Experimental Thermal and Fluid Science*, **31**, pp. 761–769, 2006.
[7] Shannak, B., Al-Shannag, M., and Al-Anber, Z. A., Gas-liquid pressure drop in vertically wavy 90° bend. *Experimental Thermal and Fluid Science*, **33**, pp. 340–347, 2009.
[8] Abdulkadir, M., D. Zhao, Azzi, A., Lowndes, I. S. and Azzopardi, B. J., Two phase air-water flow through a large diameter vertical 180° return bend. *Chemical Engineering Science*,**79**, pp. 138–152, 2012.
[9] Da Silva, M.J., Thiele, S., Abdulkareem, L., Azzopardi, B.J., and Hampel, U., High resolution gas-oil two-phase flow visualization with a capacitance wire mesh sensor. *Flow Measurement and Instrumentation*, **21**, pp. 191–197, 2010.